Michael Anibal Macías Pro[1*], Gustavo Alejandro Altamirano Briones[2], Erika Jahaira Góngora Muñoz[2], Alex Ariel Fernández Andrade[1, 3] and Kevin Jhon Fernández Andrade[1, 3]

[1] Laboratorio de Análisis Químicos y Biotecnológicos, Instituto de Investigación, Universidad Técnica de Manabí. Portoviejo, Ecuador.
[2] Departamento de Química, Facultad de Ciencias Básicas, Universidad Técnica de Manabí. Portoviejo, Ecuador. erika.gongora@utm.edu.ec - gustavo.altamirano@utm.edu.ec
[3] Departamento de Ingeniería en Maderas, Facultad de Ingeniería, Universidad del Bío-Bío, Concepción, Chile. alex.fernandez2201@alumnos.ubiobio.cl - kevin.fernandez2101@alumnos.ubiobio.cl

*Corresponding author: michael.macias@utm.edu.ec

Received: 16/08/2023. **Last review:** 23/10/2023. **Accepted:** 14/12/2023.

Adsorption of Brilliant blue FCF (B1) and Allura Red (R40) colorants on cocoa shell: kinetics of the process

Abstract

The use of dyes in food industrial processes is limited due to significant pollution in aquatic receptors from their wastewater. To address this issue, this study focused on evaluating the adsorption of dyes Allura Red (R40) and Brilliant blue FCF (B1) using cocoa shells (CS) as an absorbent. To achieve this, a pre-treatment was applied, which involved washing, grinding and drying at a temperature of 80 °C for 24 h, followed by a sieving process. The effect of the adsorbent dose was then analyzed and it was calculated that the optimal dose was 4 g/L. Additionally, the effect of contact time was studied through a kinetic analysis, all tests were carried out at a pH level of 2. The obtained data were fitted to kinetic models, which allowed us to conclude that the adsorption kinetics fit two different models depending on the initial solution conditions, in a range from 0 to 0.1512 mmol/L. Specifically, the Pseudo Second-Order (PSO) model fitted R40, while the Elovich model was appropriate for B1. In summary, CS was found to be a viable adsorbent for dyes in contaminated waters.

Keywords: Allura Red; Brilliant blue; adsorption; batch adsorption; cocoa shell.

Adsorción de los colorantes azul brillante FCF (B1) y rojo allura (R40) en cáscara de cacao: cinética del proceso

Resumen

El uso de colorantes en procesos industriales alimentarios es limitado debido a la considerable contaminación que generan en los cuerpos acuáticos que son receptores de sus efluentes residuales. Con el objetivo de abordar esta problemática, se llevó a cabo un estudio enfocado en la evaluación de la adsorción de los colorantes Rojo allura (R40) y azul brillante FCF (B1), utilizando cáscara de cacao (CS) como adsorbente. Para lograrlo, primero se aplicó un pretratamiento que comprendió diversas etapas, tales como limpieza, trituración, lavado y secado a 80 °C durante 24 h, seguido de un proceso de tamizado. Después se procedió a analizar el efecto de la dosis de adsorbente y se determinó que la dosis óptima del adsorbente era de 4 g/L. Así mismo, se estudió el efecto del tiempo de contacto a través de un estudio cinético, todos los ensayos se llevaron a cabo a un nivel de pH de 2. Los datos obtenidos fueron ajustados a modelos cinéticos, lo que permitió concluir que la cinética de adsorción se ajusta a dos modelos distintos dependiendo de las condiciones de la solución inicial, en un intervalo que va desde 0 hasta 0,1512 mmol/L. Específicamente, el modelo de pseudo segundo orden (PSO) se ajustó al colorante R40, mientras que el modelo de Elovich fue el adecuado para el colorante B1. En resumen, la CS fue viable como adsorbente para colorantes en aguas contaminadas.

Palabras clave: Rojo allura; azul brillante; adsorción; adsorción por lotes; cáscara de cacao.

Adsorção dos corantes azul brilhante FCF (B1) e vermelho allura (R40) na casca de cacau: cinética do processo

Resumo

O uso de corantes em processos industriais de alimentos é limitado devido à considerável contaminação que geram nos corpos aquáticos receptores de seus efluentes residuais. Com o objetivo de abordar este problema, foi realizado um estudo focado na avaliação da adsorção dos corantes vermelho allura (R40) e azul brilhante FCF (B1), utilizando casca de cacau (CS) como adsorvente. Para isso, foi inicialmente aplicado um pré-tratamento que incluiu várias etapas, como limpeza, moagem, lavagem e secagem a 80 °C durante 24 h, seguido de um processo de peneiramento. O efeito da dose do adsorvente foi então analisado e determinou-se que a dose ideal do adsorvente era de 4 g/L. Da mesma forma, o efeito do tempo de contato foi estudado através de um estudo cinético, todos os testes foram realizados em um nível de pH de 2. Os dados obtidos foram ajustados a modelos cinéticos, o que permitiu concluir que a cinética de adsorção se ajusta a dois modelos diferentes dependendo das condições da solução inicial, num intervalo que varia de 0 a 0,1512 mmol/L. Especificamente, o modelo de pseudo-segunda ordem (PSO) ajustou-se ao corante R40, enquanto o modelo Elovich foi adequado ao corante B1. Em resumo, o CS mostrou-se viável como adsorvente de corantes em águas contaminadas.

Palavras-chave: vermelho allura; azul brilhante; adsorção; adsorção em lote; casca de cacau.

Introduction

Artificial colorants are widely used in the food industry due to their high stability and low cost. However, their use is increasingly restricted due to the potentially toxic effects they can have on human health [1]. Industrial wastewater is often discharged with treatments that do not remove the colorants present in these matrices [2]. The concentration of colorants can reach up to 200 ppm, as approximately 15% of the utilized colorants are wasted [3].

Many studies have been conducted to evaluate the toxic effects of these colorants, with particular emphasis on Brilliant blue FCF (B1), Tartrazine and Allura Red (R40), which are among the most common ones. According to Oyewole and Oladele, prolonged exposure to these colorants can lead to impairment of cardiac and renal functions and genetic modifications [4]. The main environmental impact, as stated by Lellis *et al.*, is the inhibition of photosynthetic processes that occur on the underwater surface due to the disruption of normal light penetration [5].

Various research efforts have been made to mitigate the pollution caused by colorants, including technologies such as advanced oxidative processes [6], microbiological degradation [7] and adsorption [8]. Significant progress has been achieved with these technologies. However, the costs and operational time remain a significant challenge that has yet to be overcome. Adsorption, despite being one of the more traditional methods, stands out as one of the most attractive approaches, particularly when using bioadsorbents, which minimize operational costs and facilitate handling [9–11].

Bioadsorbents of agroindustrial origin have good chemical stability and great adsorbent performance. It has generally been taken as waste from processes where it had not been taken advantage of and entailed a final disposal problem. Among the most used agroindustrial residues, with or without chemical treatment are rice husk and ash [12], corn cob [13], husk nuts [11], sugarcane bagasse ash [14], among others.

Cocoa shells (CS) show a good performance in the removal of contaminants, however, studies to remove dye mixtures are scarce. Due to its properties and massive generation, the use of the CS can contribute as an interesting alternative to environmental management in the food industry [15].

According to Tkaczyk *et al.*, contamination by dyes such as B1 negatively affects aquatic ecosystems [16]. This study focuses on assessing the adsorption efficiency of B1 and R40 dyes within CS, proposing it as an alternative for treating both agroindustrial waste and effluents. The primary objective is to mitigate dye-induced pollution in wastewater by presenting a sustainable and efficient solution for pollutant removal. The utilization of CS, as a natural and renewable material, underscores the study's commitment to providing an environmentally friendly alternative for the treatment of industrial wastewater.

Materials and methods

Preparation and characterization of the adsorbent and standard solutions

Waste CS were utilized, which had undergone pretreatment involving a size reduction stage. Subsequently, particles ranging between 0.595 to 0.841 mm in size were carefully selected. The chosen material was thoroughly washed with distilled water to eliminate impurities, starches, and natural colors. Finally, it was dried for 24 h at a temperature of 80 °C and stored in plastic bags to prevent moisture absorption. The moisture content at the end of the drying process was measured to be 6.5%.

The reagents B1 and R40 were obtained from Sigma Aldrich. Different synthetic solutions for B1 and R40 were prepared daily, as explained in **table 1** and stored in amber flasks. Quantification was performed using a Thermo Scientific 60S Evolution UV/VIS spectrophotometer at λ_{max} of 502 nm for R40 and 629 nm for B1, using a calibration curve in a linear concentration range from 5 to 30 ppm for B1 and from 10 to 80 ppm for R40.

The concentrations of the dyes were quantified at the beginning and end of the adsorption experiment, using a Thermo Scientific 60 S Evolution UV/VIS spectrophotometer at λ_{max} of 592 nm, by means of a calibration curve in a linear concentration range between 20 and 140 $\mathrm{mg/L}$ of standard B1.

Point of zero charge

The pH at which the surface charge of the materials becomes neutral and reaches equilibrium is known as the point of zero charge denoted as pHzc [17]. To determine the pHzc of the adsorbent, the methodology described by Villa was followed [18]. A volume of 50 mL of distilled water was measured and placed into 100 mL Erlenmeyer flasks. Subsequently, the pH of each solution was adjusted within a range between 2, 4, 6, 8, and 10 units by adding either 0.1 M HCl or 0.1 M NaOH. Then, 0.5 g of the adsorbent material sample was introduced into each of these solutions and covered with aluminum foil. Following a 48 h period, during which the solutions were continuously agitated at room temperature, the solutions underwent filtration, and the final pH values of the filtrates were reevaluated. The disparity between the initial pH values and the final pH values was plotted against the initial pH values. The point of intersection of the resulting curve with the x-axis, where this disparity equates to zero, unequivocally denotes the point of zero charge [19].

Adsorption assays

The dose of the adsorbent and the contact time were evaluated through the kinetic study. All the experiments were carried out in 250 mL Erlenmeyer flasks, where 100 mL of B1 and R40 dye solutions were placed. Aluminum foil covers were used over the flasks to prevent photodegradation. To improve the solution's contact with the adsorbent, an orbital shaker (Thermo Scientific) was used at a speed of 300 rpm as Andrade *et al.* reported [9].

All assays were carried out in triplicate at room temperature (25 °C), and pH 2, due to there are many studies reporting this pH as optimal for achieving the maximum percentage of removal [20, 21]. The dose of the adsorbent was evaluated using a solution with an initial concentration of 0.1512 mmol/L for both dyes. Different doses of CS from 0.2 to 2.0 g at 0.2 g intervals were tested over 24 h. The temperature for all tests was set at 298 K. For the investigation of contact time, seven mixture solutions with varying concentrations

Table 1. Composition of mixtures for adsorption assays.

Initial colorants concentrations in each mixture (mmol/L)							
Colorants	**M1**	**M2**	**M3**	**M4**	**M5**	**M6**	**M7**
R40	0.1512	0.1422	0.0708	0.1427	0	0.0690	0
B1	0.1514	0.0745	0.1455	0	0.1549	0	0.0748

were used for each dye: mixture one (M1), mixture two (M2), mixture three (M3), mixture four (M4), mixture five (M5), mixture six (M6) and mixture seven (M7), as shown in **table 1**.

To determine the best contact time, capacity, and percentage removal, Eq. (1) and Eq. (2) were used.

$$Q_e = \frac{(C_0 - C_t)}{w} V \quad (1)$$

$$\%R = \frac{(C_0 - C_t)}{C_0} \ 100 \quad (2)$$

Where, $Q_e\ (mmol/g)$ is the adsorption capacity, $C_0\ (mmol/L)$ is the initial concentration of adsorbate, $C_t\ (mmol/L)$ is the concentration of the adsorbate at time $t\ (min)$, $V\ (mL)$ is the volume of the solution, and $w\ (g)$ is the mass of the adsorbent. R is the percentage removal.

Kinetic study

Kinetic assays were conducted under the previously established conditions, including a solution volume of 50 mL, 4 g/L of adsorbent, and concentrations ranging from 0 to 0.01512 mmol/L, with contact times from 1 to 360 min (1, 5, 10, 15, 20, 30, 45, 60, 90, 120, 180, 240, 300, 360 min). The data obtained was fitted to nonlinear mathematical models using R Software. The kinetic models are presented in **table 2**.

Table 2. Nonlinear kinetic models.

Models	Equation	Adjustment parameter
Pseudo First-Order (PPO)	$Q_t = Q_e(1 - exp\ (k_1 t)$	Q_e: maximun adsorption capacity k_1: First-Order adsorption rate constant
Pseudo Second-Order (PSO)	$Q_t = \frac{k_2 q_e^2 t}{1 + k_2 Q_e t}$	Q_e: maximun adsorption capacity k_2: Second-Order adsorption rate constant
Elovich	$Q_t = \frac{1}{\beta} ln\ (1 + \alpha C t)$	α: chemisorption rate constant β: surface coverage extent
Bangham	$Q_t = k_r t^{1/m}$	k_r: Bangham adsorption rate constant $1/m$: adsorption density intensity
Intraparticle diffusion (ID)	$Q_t = k_{id} t^{1/2} + C$	k_{id}: intraparticle diffusion rate constant C: diffusion constant

Results and Discussion

Adsorbent Dose Effect

There is a direct relationship between the amount of adsorbent and the removal of both dyes (**figure 1**). As there is a higher dose of adsorbent, the number of active sites increases, therefore there are more spaces where these molecules can be retained [22].

This effect occurs similarly for both dyes since they are at the same concentration. It is notorious that B1 adsorbs more than R40, which can be attributed to the distinct chemical structures of both dyes. B1 possesses three sulfonate groups, a charged nitrogen and a nitrogen with a lone pair of electrons. These functional groups are prone to experiencing stronger intermolecular interactions with the adsorbent [23, 24].

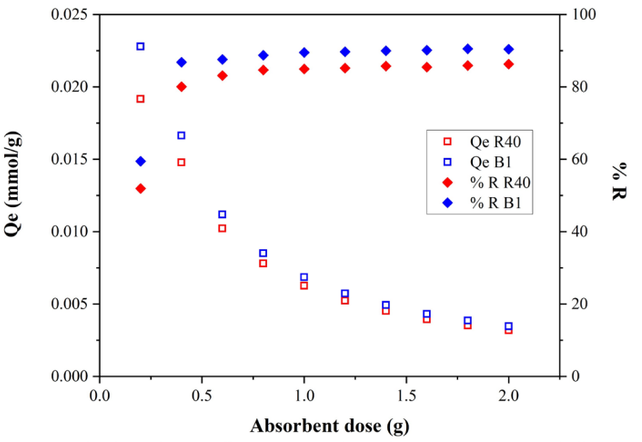

Figure 1. Adsorbent dosage effect on R40 and B1 adsorption onto cocoa shells.

In contrast, the R40 molecule features two sulfonate groups, and its nitrogens are part of an azo compound. These groups exhibit greater steric hindrance due to the aromatic rings, thereby impeding a strong interaction with the functional groups of the adsorbent [25-27]. The %R increased faster until the dose of 4 g/L, then variation was minimal and almost constant, for this reason, it was established as a dose of adsorbent.

Material characterization

Fourier-transform infrared (FT-IR) spectroscopy was employed to identify potential functional groups responsible for adsorption. As a result, a broad signal in the range of 3200 to 3600 cm^{-1} was observed (**figure 2A**), corresponding to hydrogen bonding interactions in –OH groups. Additionally, the presence of aliphatic C–H bonds was evidenced by the signal at 2918 cm^{-1}. Vibrations of aromatic ring C=C bonds were observed at 1601 cm^{-1}. Furthermore, signals recorded at 1024 cm^{-1} correspond to angular deformations in the C–O bond. Taken together, these findings lead to the conclusion that the material possesses phenolic groups, which are responsible for the adsorption processes.

Point of zero charge

The obtained values are presented in **figure 2B**. The calculated pHzc value was 7.5, this value indicates a state of charge equilibrium on the adsorbent material, whereby pH levels above 7.5 result in a negatively charged surface, while pH levels below 7.5 lead to a positively charged surface. Notably, at pH 2.0, B1 exhibits a negative charge in its sulfonate group, whereas R40 does not possess any negative charges. This observation allows us to deduce that B1 is adsorbed in larger quantities than R40.

Effect of contact time

The concentration decreased rapidly during the first few minutes, reaching equilibrium at 120 min for M1-R40, M1-B1, M2-R40, M2-B1, M3-R40, M3-B1 (**figure 3**) and for M4-R40, M5-B1, M6-R40, M7-B1 (**figure 4**). In the case of M5-B1, equilibrium was reached at 150 min (**figure 4B**).

In the case of M1 (**figures 3A and 3B**), the concentrations of R40 and B1 were equal (0.1512 mmol/L), resulting in an equal distribution of active sites and similar maximum adsorption values (0.01248 and 0.01280 mmol/g). Both dyes showed an affinity for the adsorbent; however, B1 exhibited a superior adsorption capacity.

For M2 (**figures 3C** and **3D**), the concentrations used were 0.1512 and 0.0746 mmol/L for R40 and B1, respectively. In this case, the adsorption capacity was higher for the component with a higher initial solution concentration (R40, 0.01469 mmol/g > B1, 0.00773 mmol/g). This can be attributed to the fact that a higher number

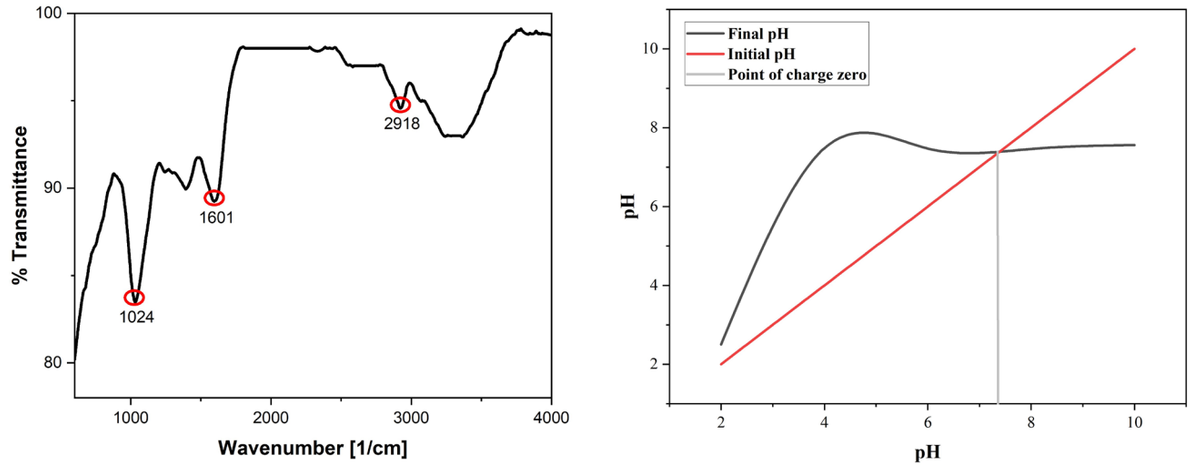

Figure 2. A: FTIR spectra of cocoa shells and B: point of zero charge of cocoa shells (pH at surface charge neutrality).

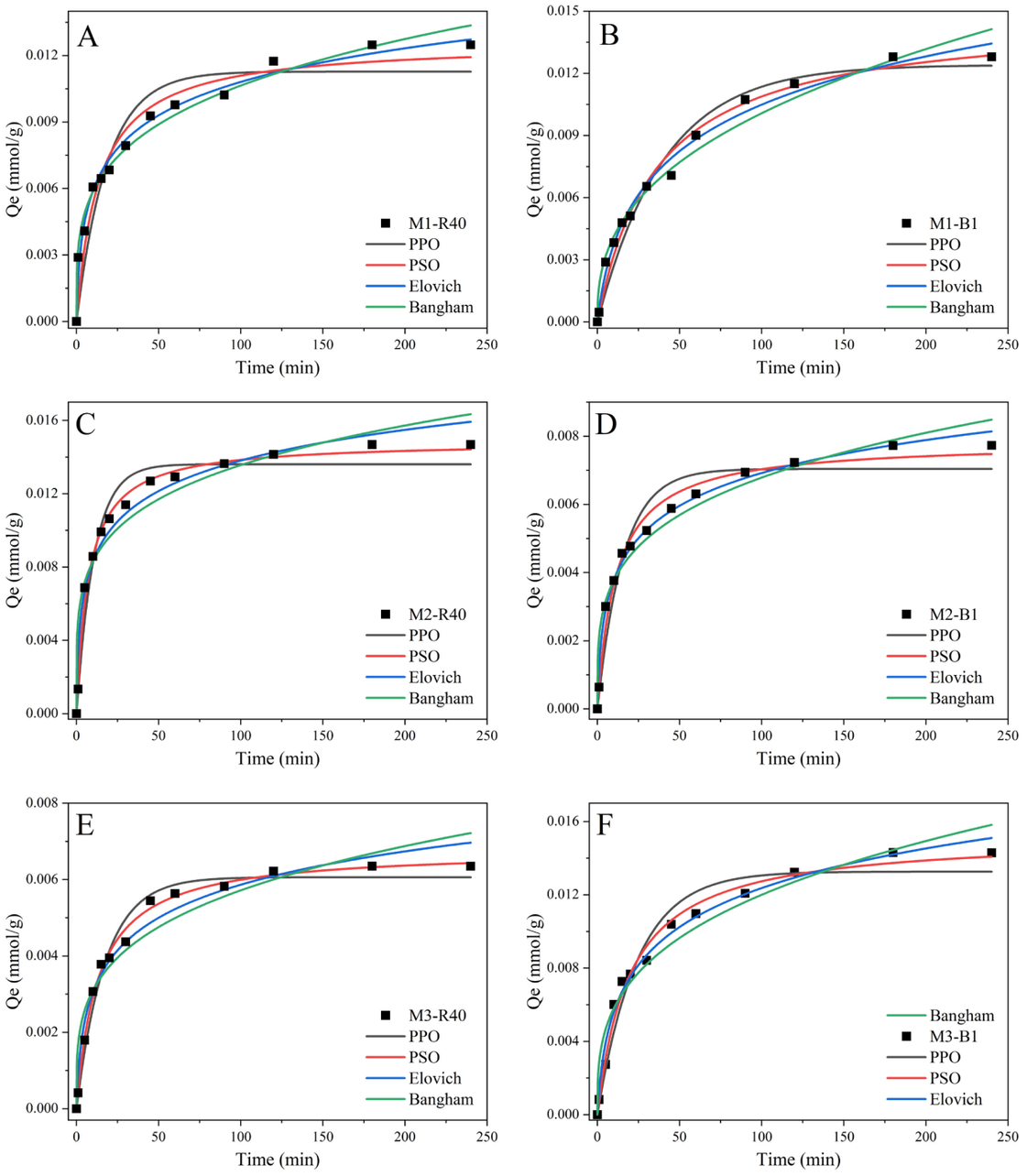

Figure 3. Kinetic models fitted to experimental data: Pseudo First-Order (PPO) Pseudo Second-Order (PSO) Elovich Bangham
M: mixtures, R40: Allura Red, B1: Brilliant blue. A: M1-R40; B: M1-B1; C: M2-R40; D: M2-B1; E: M3-R40; and F: M3-B1.

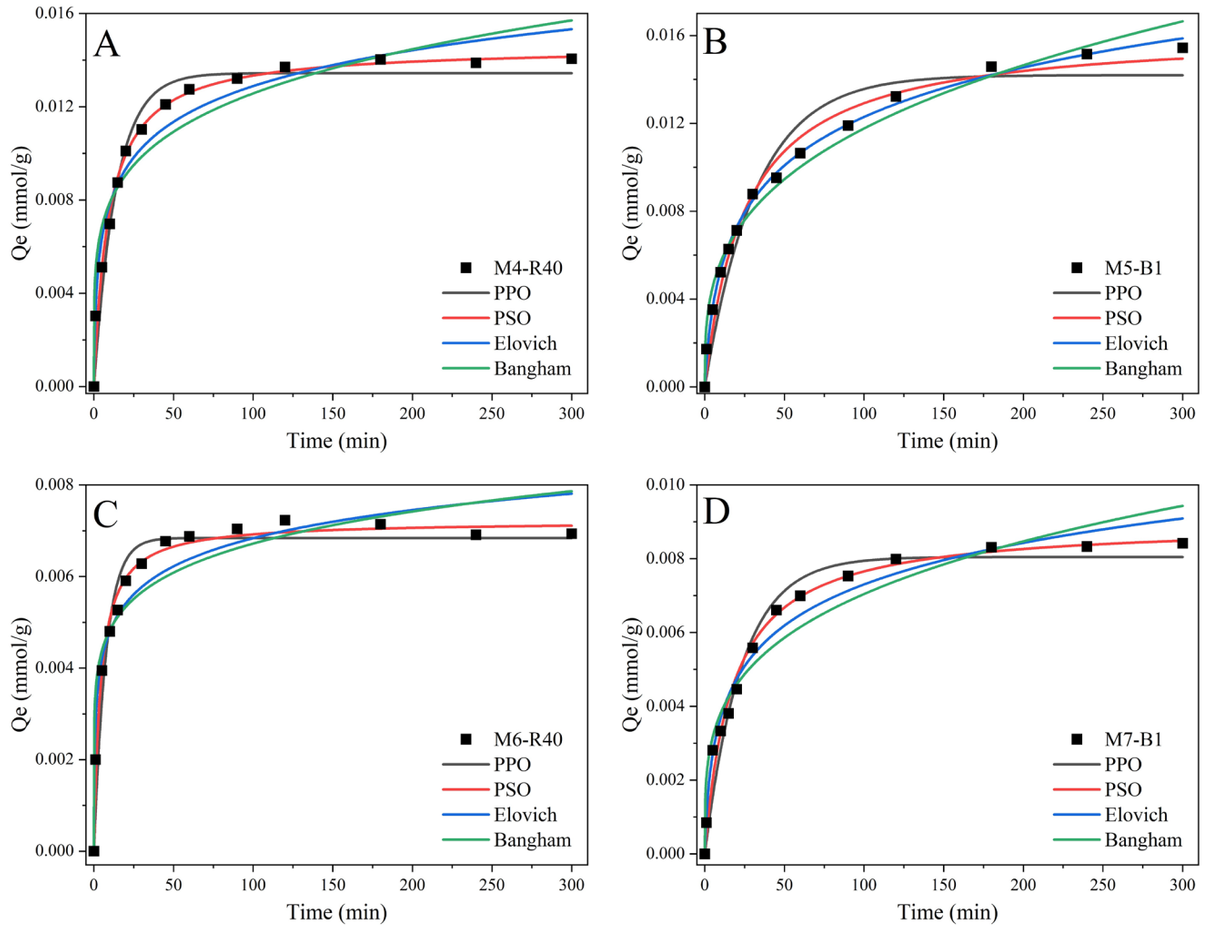

Figure 4. Kinetic models fitted to experimental data: Pseudo First-Order (PPO) ——— Pseudo Second-Order (PSO) ——— Elovich ——— Bangham ———
M: mixtures, R40: Allura Red, B1: Brilliant blue. A: M1-R40; B: M1-B1; C: M2-R40; D: M2-B1; E: M3-R40; and F: M3-B1.

of molecules leads to stronger interactions between the adsorbate and adsorbent.

The same effect is observed in M3 (**figures 3E** and **3F**), where the adsorption capacity was higher for B1 (0.01429 mmol/g) compared to R40 (0.00635 mmol/g). This is because B1 concentration (0.1512 mmol/L) in M3 was higher than R40 (0.0746 mmol/L).

In assays M4 (**figure 4A**) and M6 (**figure 4C**), where only the R40 dye was used at concentrations of 0.1427 mmol/L and 0.690 mmol/L, respectively, the reported adsorption capacity is not significantly different from that shown in trials M2 (**figure 3C**) and M3 (**figure 3E**), despite the latter two being in competition with B1. This demonstrates that the adsorption capacity of R40 is not strongly influenced or compromised when combined with B1.

Finally, in assays M5 (**figure 4B**) and M7 (**figure 4D**) concentrations of B1 dye at 0.1549 mmol/L and 0.0748 mmol/L were used, respectively, which are similar to those employed in trials M2 (**figure 3D**) and M3 (**figure 3F**). In these trials, a higher adsorption capacity was evidenced. This improvement in adsorption capacity is attributed to the presence of a single dye in each trial, which avoids competition for active sites on the adsorbent, allowing for greater efficiency in the adsorption process.

In **figure 5** it can be observed that B1 consistently shows higher adsorption capacity than R40 in all cases. Assay M7 shown a higher dye removal for B1, assay M6 had a better dye removal for R40, and the assay M2 shown a better dye removal when dyes were mixed.

Kinetic study

The fitting parameters of the Pseudo First-Order (PPO), Pseudo Second-Order (PSO), Elovich, and Bangham and Intraparticle Difusion (ID) kinetic models used are shown in **table 3**, **table 4**, **figure 3**, **figure 4**, **figure 6** and **figure 7**. The goodness of fit was evaluated using the Residual Standard Error (RSE) and the model with the lowest RSE indicates the best fit.

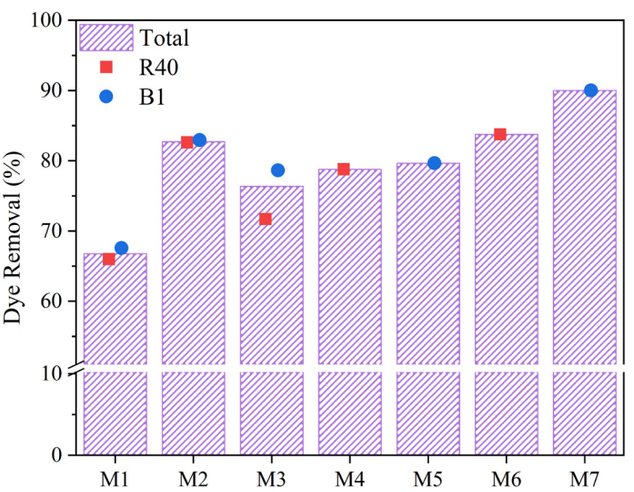

Figure 5. Comparative boxplot assays dyes removal (%).

The experimental data did not fit the PPO or Bangham models, as the calculated values had higher errors (**table 3**). The intraparticle diffusion model was applied to gain a deeper insight into the adsorption mechanism. A proper fit of this model indicates the predominant adsorption mechanism.

Table 3. Kinetic constants of R40 and B1 dye adsorption on cocoa shells.

	M1		M2		M3		M4	M5	M6	M7
	R40	B1	R40	B1	R40	B1	R40	B1	R40	B1
Qe,exp (mmol/g)	0.0125	0.0128	0.0147	0.0077	0.0064	0.0143	0.0141	0.0154	0.0069	0.0084
PPO										
Qe,cal (mmol/g^1)	0.0113	0.0124	0.0136	0.007	0.0061	0.0133	0.0134	0.0142	0.0068	0.0081
K_1 (min^{-1})	0.0535	0.0247	0.0933	0.0639	0.0572	0.0415	0.0719	0.0312	0.1314	0.0433
R^2	0.9034	0.9703	0.9654	0.9466	0.9819	0.9657	0.9692	0.9527	0.9536	0.9728
χ^2	1.54×10−6	6.25×10−7	8.78×10−7	3.68×10−7	9.66×10−8	8.87×10−7	6.88×10−7	1.29×10−6	2.39×10−7	2.40×10−7
PSO										
Qe,cal (mmol/g)	0.0126	0.0148	0.0149	0.0078	0.0068	0.0152	0.0146	0.0162	0.0072	0.009
K_2 (g/mmol.min)	5.786	1.878	9.168	11.126	11.165	3.342	7.349	2.406	33.17	6.481
R^2	0.9537	0.9852	0.9941	0.986	0.9955	0.9901	0.9883	0.985	0.987	0.9897
χ^2	7.39×10−7	3.12×10−7	1.50×10−7	9.63×10−8	2.42 × 10−8	2.57 × 10−7	2.60×10−7	4.09×10−7	6.72×10−8	9.06×10−8
Elovich										
α (g/mmol.min)	0.003	0.0007	0.0073	0.0019	0.0013	0.0016	0.0073	0.0013	0.0198	0.0014
β (g/mmol)	454.8	287	413.6	713.4	789.3	316.3	450	302.4	1128.4	610.7
R^2	0.9869	0.9902	0.9718	0.9917	0.9745	0.9889	0.9684	0.9968	0.9466	0.9805
χ^2	2.09×10−7	2.06×10−7	7.17×10−7	5.71×10−8	1.36×10−7	2.87×10−7	7.05×10−7	8.66×10−8	3.30×10−6	1.72×10−7
Bangham										
K_r (g mmol/ g.min)	0.0032	0.0017	0.0051	0.0021	0.0017	0.3156	0.005	0.0028	0.0035	0.0021
A (g/mmolmin)	0.2597	0.3868	0.2131	0.2553	0.266	0.0028	0.2024	0.3155	0.1431	0.266
R^2	0.9852	0.9746	0.9203	0.9553	0.9236	0.9546	0.9283	0.9815	0.9066	0.9431
χ^2	2.36×10−7	5.35×10−7	2.02×10−6	3.08×10−7	4.08×10−7	1.18×10−6	1.60×10−6	5.07×10−7	4.81×10−7	5.01×10−7

PPO: Pseudo First-Order
PSO: Pseudo Second-Order
Qe,exp: maximum adsorption capacity
Qe,cal: maximum adsorption capacity
K_1: First-Order adsorption rate constant
K_2: Second-Order adsorption rate constant
α: chemisorption rate constant
β: surface coverage extent
K_r: Bangham adsorption rate constant
A: adsorption density intensity
R^2: coefficient of determination
χ^2: Chi square

The graphical representation of the model Weber-Morris in function of time (t) (Qt vs. t0.5) displays three regions with linear relationships (**figure 6** and **figure 7**). This suggests that when some stages intersect at the origin, the process is solely governed by intraparticle diffusion. However, if the experimental data exhibits multilinearity, it indicates that the adsorption process may be controlled by multiple steps or a combination of them. Nevertheless, in our study, none of the three stages passes through the origin. This finding is crucial as it suggests that intraparticle diffusion does not serve as the limiting stage in the adsorption process.

The kinetic data for R40 had a better fit to the PSO model, while B1 showed a better fit to the Elovich model. This means that both dyes are adsorbed differently, and it could partially explain the higher affinity of B1 for the adsorbent. However, the type of adsorption varies depending on the initial concentrations of each dye.

On the one hand, the fact that the kinetics fit the PSO model indicates that at pH 2, in R40, there are no charges present, and adsorption occurs through electrons donated by nitrogen atoms. On the other hand, in B1, there are formal charges on the sulfonate group that can exhibit a strong electrostatic attraction with the material. If it fits the Elovich model, it indicates that the process involves chemisorption and depends on the bonds formed between the adsorbate and the adsorbent. Both models are related to the type of adsorption occurring in the process, which explains why the kinetic data fit differently when the initial concentrations of the dyes are changed.

Furthermore, the Elovich model is related to the heterogeneity and activation energy of the CS surface. The parameter β, which is related to the extent of surface coverage and activation energy [9], showed an inverse relationship with the initial concentration of B1 in the presence of higher concentrations of R40. Thus, the presence of a higher proportion of R40 saturates the active sites of the adsorbent, preventing the accommodation of B1 molecules present in lower amounts. This explains why the adsorption capacity is higher for the dye with a higher concentration.

The parameter α is related to the adsorption rate and is therefore related to the K_2 constant of the PSO model. Observing its values (**table 4**), it can be seen that they have a direct relationship with the initial concentrations of the dyes. Additionally, these values increase even more when the dye of interest is present at a higher

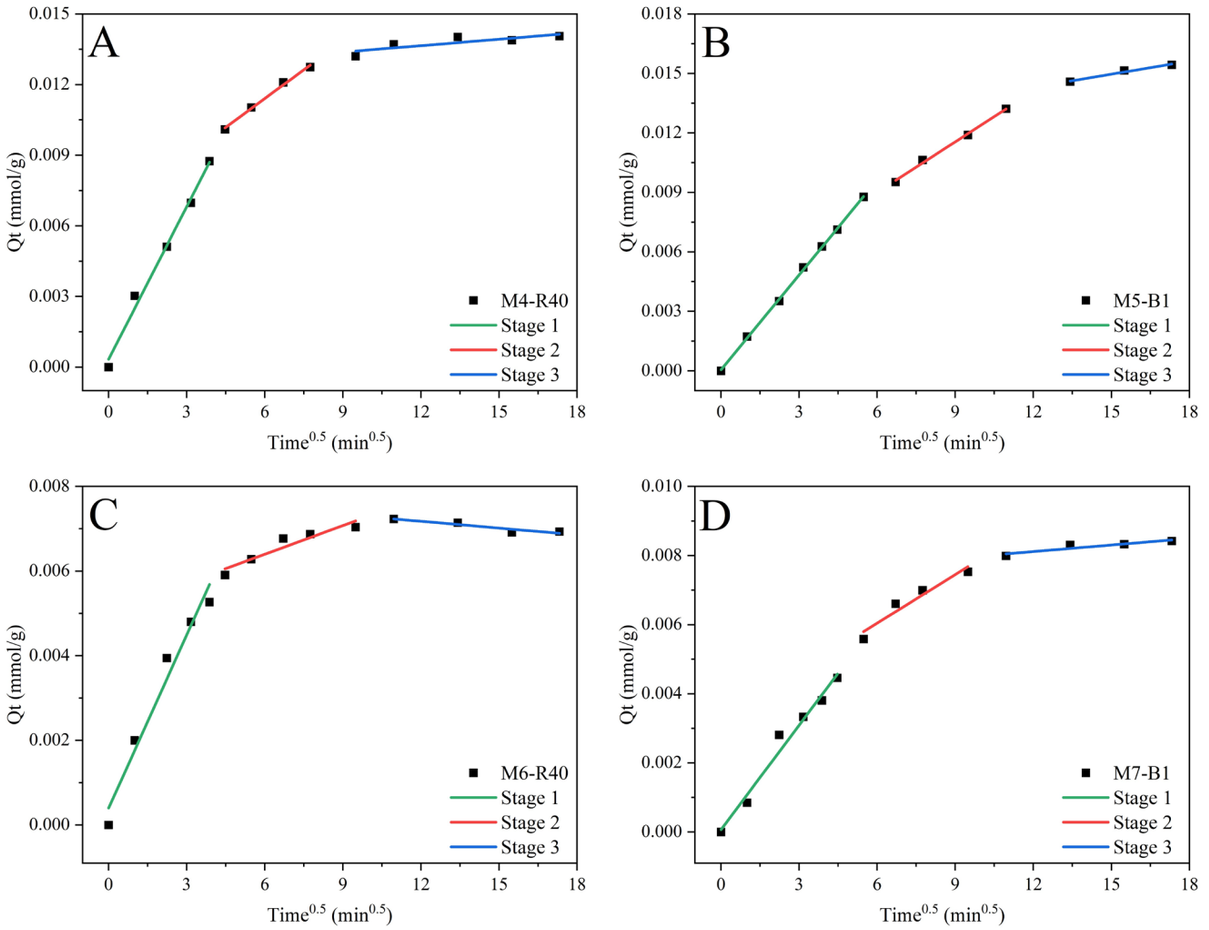

Figure 6. Weber-Morris intraparticle diffusion model adjusted to experimental data. M: mixtures, R40: Allura Red, B1: Brilliant blue. A: M1-R40; B: M1-B1; C: M2-R40; D: M2-B1; E: M3-R40; and F: M3-B1.

concentration and with the presence (low concentration) of the other dye. Despite the equal distribution of active sites for both dyes, the adsorption process occurs competitively. The results obtained indicate that the presence of aliphatic or aromatic OH groups is responsible for the adsorption process. The B1 molecule, which carries a positive charge at the tested pH levels, is favored in the experiments. This preference is attributed to the interaction between the unshared electron pairs of oxygen and the positively charged regions in the dye's structure.

Table 4. Kinetic constants for Weber-Morris Intraparticle Diffusion model in R40 and B1 dye adsorption on cocoa shells.

	M1		M2		M3		M4	M5	M6	M7
	R40	B1	R40	B1	R40	B1	R40	B1	R40	B1
Stage 1										
K_{id} (mmol/g.min0.5)	0.00179	0.00109	0.00313	0.00137	0.00082	0.00124	0.00216	0.00160	0.00136	0.00101
C (mmol/g)	0.00039	0.00016	-0.00064	-0.00026	-0.00014	-0.00015	0.00034	0.00005	0.00040	0.00007
R^2	0.91472	0.99357	0.92499	0.93408	0.94341	0.97314	0.99069	0.99930	0.96632	0.97781
Stage 2										
K_{id} (mmol/g.min0.5)	0.00073	0.00000	0.00093	0.00043	0.00045	0.00091	0.00081	0.00085	0.00023	0.00047
C (mmol/g)	0.00381	0.01280	0.00615	0.00279	0.00195	0.00361	0.00652	0.00392	0.00504	0.00324
R^2	0.95329	1.00000	0.94986	0.96825	0.92214	0.97851	0.99365	0.99555	0.89229	0.93245
Stage 3										
K_{id} (mmol/g.min0.5)	0.00017	0.00000	0.00018	0.00000	0.00003	-0.00001	0.00009	0.00022	-0.00005	0.00006
C (mmol/g)	0.0102	0.00000	0.01212	0.00771	0.00045	0.01443	0.01257	0.01168	0.00782	0.00736
R^2	0.79127	0.00000	0.86688	1.00000	0.77771	1.00000	0.70422	0.97596	0.86903	0.85109

K_{id}: intraparticle diffusion rate constant
C: diffusion constant
R^2: coefficient of determination

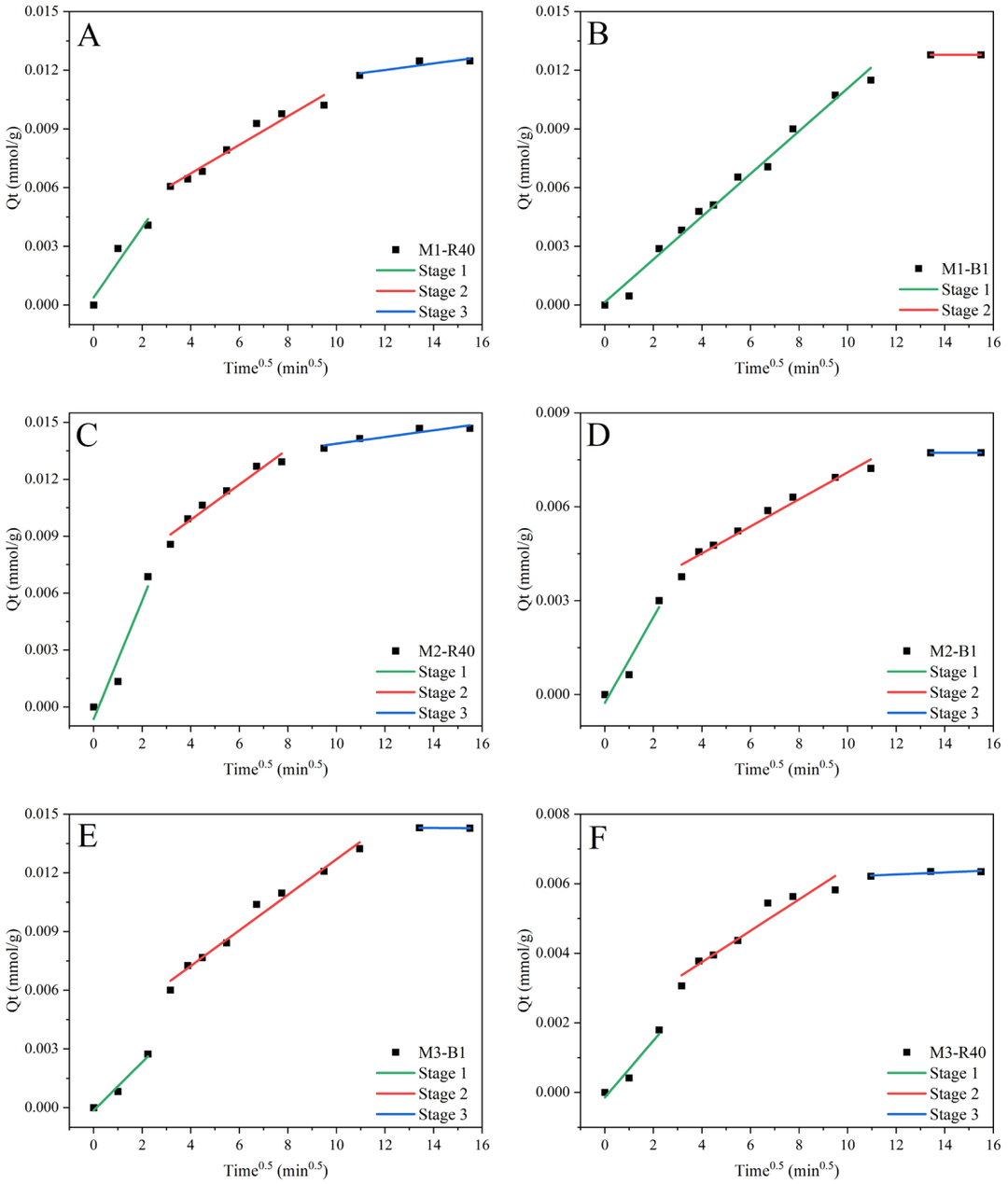

Figure 7. Weber-Morris intraparticle diffusion model adjusted to experimental data. M: mixtures, R40: Allura Red, B1: Brilliant blue. A: M1-R40; B: M1-B1; C: M2-R40; D: M2-B1; E: M3-R40; and F: M3-B1.

Conclusions

It was determined that the adsorption behavior of both dyes was influenced by their concentration. The well-fitting kinetic data with the PSO and Elovich models suggests that the adsorption process occurs through chemical mechanisms. This highlights the crucial influence of each dye's chemical structure on its adsorption capacity and affinity. Notably, B1 showed higher adsorption than R40 at the same concentration, attributed to distinct chemical structures. Both dyes exhibited similar adsorption behavior when their initial concentrations were equal, indicating that the process occurs equally for both. Despite this similarity, remarkably high percentages of adsorption were achieved for the dye mixture.

This study showed that the adsorption capacity of dyes is usually higher in single-component systems compared to two-component systems. This is due to the different affinities presented by the dyes with the adsorbent, resulting in competition between them and affecting the efficiency of removal. Furthermore, it is observed that removal in two-component systems is influenced by the individual percentages of the dyes in the mixtures to be treated. However, in this study and under the specific experimental conditions employed, it was observed that the differences in removal percentages between single-component and two-component systems were not as pronounced as anticipated.

References

[1] M. Ng Hau Kwan, C. P. Leo, S. M. N. Arosa Senanayake, G. K. Lim and M. K. Tan, "Carbon-dot dispersal in PVA thin film for food colorant sensing", *J Environ Chem Eng*, vol. 8, no. 3, pp. 1–6, 2020. DOI: https://doi.org/10.1016/j.jece.2019.103187

[2] X. Wang, J. Jiang and W. Gao, "Reviewing textile wastewater produced by industries: characteristics, environmental impacts, and treatment strategies", *Water Science and Technology*, vol. 85, no. 7, pp. 2076–2096, Mar. 2022. DOI: https://doi.org/10.2166/wst.2022.088

[3] M. R. Hossain, T. U. Rashid, N. P. Lata, S. C. Dey, M. Sarker and S. Md. Shamsuddin, "Fabrication of Novel Nanohybrid Material

for the Removal of Azo Dyes from Wastewater", *Journal of Composites Science*, vol. 6, no. 10, pp. 1–21, 2022. DOI: https://doi.org/10.3390/jcs6100304

[4] O. I. Oyewole and J. O. Oladele, "Assessment of Cardiac and Renal Functions in Wistar Albino Rats Administered Carmoisine and Tartrazine", *Adv Biochem*, vol. 4, no. 3, pp. 21–25, Jun. 2016. DOI: https://doi.org/10.11648/j.ab.20160403.11

[5] B. Lellis, C. Z. Fávaro-Polonio, J. A. Pamphile and J. C. Polonio, "Effects of textile dyes on health and the environment and bioremediation potential of living organisms", *Biotechnology Research and Innovation*, vol. 3, no. 2, pp. 275–290, 2019. DOI: https://doi.org/10.1016/j.biori.2019.09.001

[6] R. M. da R. Santana *et al*., "Degradation of Textile Dyes Employing Advanced Oxidative Processes: Kinetic, Equilibrium Modeling, and Toxicity Study of Seeds and Bacteria", *Water Air Soil Pollut*, vol. 230, no. 6, pp. 1–13, 2019. DOI: https://doi.org/10.1007/s11270-019-4178-x

[7] Z. Ghobadi Nejad, S. M. Borghei and S. Yaghmaei, "Biodegradation of synthetic dye using partially purified and characterized laccase and its proposed mechanism", *International Journal of Environmental Science and Technology*, vol. 16, no. 12, pp. 7805–7816, 2019. DOI: https://doi.org/10.1007/s13762-019-02226-5

[8] T.-S. Kim, H. J. Song, M. A. Dar, H.-J. Lee and D.-W. Kim, "Fast adsorption kinetics of highly dispersed ultrafine nickel/carbon nanoparticles for organic dye removal", *Appl Surf Sci*, vol. 439, pp. 364–370, 2018. DOI: https://doi.org/10.1016/j.apsusc.2018.01.061

[9] C. A. Andrade, L. A. Zambrano-Intriago, N. S. Oliveira, J. S. Vieira, L. S. Quiroz-Fernández and J. M. Rodríguez-Díaz, "Adsorption Behavior and Mechanism of Oxytetracycline on Rice Husk Ash: Kinetics, Equilibrium, and Thermodynamics of the Process", *Water Air Soil Pollut*, vol. 231, no. 3, pp. 1–16, 2020. DOI: https://doi.org/10.1007/s11270-020-04473-6

[10] Z. Shamsollahi and A. Partovinia, "Recent advances on pollutants removal by rice husk as a bio-based adsorbent: A critical review", *J Environ Manage*, vol. 246, pp. 314–323, 2019. DOI: https://doi.org/10.1016/j.jenvman.2019.05.145

[11] M. Banerjee, R. K. Basu and S. K. Das, "Cr(VI) adsorption by a green adsorbent walnut shell: Adsorption studies, regeneration studies, scale-up design and economic feasibility", *Process Safety and Environmental Protection*, vol. 116, pp. 693–702, 2018. DOI: https://doi.org/10.1016/j.psep.2018.03.037

[12] J. F. Honorio, M. T. Veit, P. Y. R. Suzaki, P. F. Coldebella, E. S. Rigobello and C. R. G. Tavares, "Adsorption of naturals hormones estrone, 17β-estradiol, and estriol by rice husk: monocomponent and multicomponent kinetics and equilibrium", *Environ Technol*, vol. 41, no. 9, pp. 1075–1092, 2020. DOI: https://doi.org/10.1080/09593330.2018.1521472

[13] C. Tejada-Tovar M.Sc., A. Herrera-Barros Ph.D. and A. Villabona-Ortíz M.Sc., "Assessment of Chemically Modified Lignocellulose Waste for the Adsorption of Cr (VI)", *Revista Facultad de Ingeniería*, vol. 29, no. 54, pp. 1–18, 2020. DOI: https://doi.org/10.19053/01211129.v29.n54.2020.10298

[14] J. M. Rodríguez-Díaz, J. O. P. García, L. R. B. Sánchez, M. G. C. da Silva, V. L. da Silva and L. E. Arteaga-Pérez, "Comprehensive Characterization of Sugarcane Bagasse Ash for Its Use as an Adsorbent", *Bioenergy Res*, vol. 8, no. 4, pp. 1885–1895, 2015. DOI: https://doi.org/10.1007/s12155-015-9646-6

[15] G. Rodríguez-Arellano, J. Barajas-Fernández, R. García-Alamilla, L. M. Lagunes-Gálvez, A. H. Lara-Rivera and P. García-Alamilla, "Evaluation of Cocoa Beans Shell Powder as a Bioadsorbent of Congo Red Dye Aqueous Solutions", *Materials*, vol. 14, no. 11, 2021. DOI: https://doi.org/10.3390/ma14112763

[16] A. Tkaczyk, K. Mitrowska and A. Posyniak, "Synthetic organic dyes as contaminants of the aquatic environment and their implications for ecosystems: A review", *Science of The Total Environment*, vol. 717, pp.1–13, 2020. DOI: https://doi.org/10.1016/j.scitotenv.2020.137222

[17] A. Tămaş, I. Cozma, L. Cocheci, L. Lupa and G. Rusu, "Adsorption of Orange II Onto Zn2Al–Layered Double Hydroxide Prepared From Zinc Ash", *Front Chem*, vol. 8, 2020. DOI: https://doi.org/10.3389/fchem.2020.573535

[18] F. A. Amaringo Villa, "Determinación del punto de carga cero y punto isoeléctrico de dos residuos agrícolas y su aplicación en la remoción de colorantes", *Revista de Investigación Agraria y Ambiental*, vol. 4, no. 2, pp. 27–36, Oct. 2013. DOI: https://doi.org/10.22490/21456453.982

[19] L. D. Hafshejani *et al*., "Removal of zinc and lead from aqueous solution by nanostructured cedar leaf ash as biosorbent", *J Mol Liq*, vol. 211, pp. 448–456, 2015. DOI: https://doi.org/10.1016/j.molliq.2015.07.044

[20] K. Litefti, M. S. Freire, M. Stitou and J. González-Álvarez, "Adsorption of an anionic dye (Congo red) from aqueous solutions by pine bark", *Sci Rep*, vol. 9, no. 1, pp. 1–13, 2019. DOI: https://doi.org/10.1038/s41598-019-53046-z

[21] B. H. Hameed, A. A. Ahmad and N. Aziz, "Adsorption of reactive dye on palm-oil industry waste: Equilibrium, kinetic and thermodynamic studies", *Desalination*, vol. 247, no. 1, pp. 551–560, 2009. DOI: https://doi.org/10.1016/j.desal.2008.08.005

[22] A. Roy, "Removal of color from real textile dyeing effluent utilizing tannin immobilized jute fiber as biosorbent: optimization with response surface methodology", *Environmental Science and Pollution Research*, vol. 28, no. 10, pp. 12011–12025, 2021. DOI: https://doi.org/10.1007/s11356-020-08820-2

[23] C. Morris, S. J. Mooney and S. D. Young, "Sorption and desorption characteristics of the dye tracer, Brilliant Blue FCF, in sandy and clay soils", *Geoderma*, vol. 146, no. 3, pp. 434–438, 2008. DOI: https://doi.org/10.1016/j.geoderma.2008.06.021

[24] EFSA Panel on Food Additives and N. S. added to Food (ANS), "Scientific Opinion on the re-evaluation of Brilliant Blue FCF (E 133) as a food additive", *EFSA Journal*, vol. 8, no. 11, pp. 1–36, 2010. DOI: https://doi.org/10.2903/j.efsa.2010.1853

[25] R. G. Sánchez-Duarte, D. I. Sánchez-Machado, J. López-Cervantes and Ma. A. Correa-Murrieta, "Adsorption of allura red dye by cross-linked chitosan from shrimp waste", *Water Science and Technology*, vol. 65, no. 4, pp. 618–623, Feb. 2012. DOI: https://doi.org/10.2166/wst.2012.900

[26] A. K. Ávila-Martínez, J. H. Roque-Ruiz, J. Torres-Pérez, N. A. Medellín-Castillo and S. Y. Reyes-López, "Allura Red dye sorption onto electrospun zirconia nanofibers", *Environ Technol Innov*, vol. 18, pp. 1–13, 2020. DOI: https://doi.org/10.1016/j.eti.2020.100760

[27] B. Takam, E. Acayanka, G. Y. Kamgang, M. T. Pedekwang and S. Laminsi, "Enhancement of sorption capacity of cocoa shell biomass modified with non-thermal plasma for removal of both cationic and anionic dyes from aqueous solution", *Environmental Science and Pollution Research*, vol. 24, no. 20, pp. 16958–16970, 2017. DOI: https://doi.org/10.1007/s11356-017-9328-3

Citación del artículo:

M. A. Macías Pro, G. A. Altamirano Briones, E. J. Góngora Muñoz, A. A. Fernández Andrade and K. J. Fernández Andrade, "Adsorption of Brilliant blue FCF (B1) and Allura Red (R40) colorants on cocoa shell: kinetics of the process", *Rev. Colomb. Quim.*, vol. 52, no. 2, pp. 11–19, 2023. DOI: https://doi.org/10.15446/rev.colomb.quim.v52n2.110635